Coexistence of two adamantane binding sites in the influenza A M2 ion channel

Matthew R. Rosenberg and Marco G. Casarotto[1]

Department of Structural Biology, John Curtin School of Medical Research, Australian National University, Acton, ACT 2601, Australia

Edited* by Robert A. Lamb, Northwestern University, Evanston, IL, and approved June 25, 2010 (received for review February 23, 2010)

The influenza A virus contains a proton-selective ion channel (M2) that is the target of the adamantane family of drug inhibitors. Two recently published studies relating to adamantane binding of the M2 ion channel using X-ray crystallography and solution NMR have reignited interest in the potential use of adamantanes in combating the spread of influenza A. However, these two studies propose different binding sites for the adamantane drugs with the X-ray M2/amantadine structure favoring an ion channel pore-binding model and the solution NMR M2/rimantadine structure suggesting the existence of a lipid-facing binding pocket. We conducted a series of surface plasmon resonance (SPR) experiments designed to accurately measure the affinity of amantadine and rimantadine to M2 ion channels embedded in 1,2-dimyristoyl-sn-glycero-phosphocholine (DMPC) liposomes. We find that this class of drug is capable of binding M2 with two different affinities in the order of 10^{-4} and 10^{-7} M, suggesting that both proposed binding sites are feasible. Furthermore, by examining drug binding to M2 mutant constructs (V27A, S31N, and D44A), it was possible to probe the location of the two binding sites. We show that a high-affinity binding site corresponds to the M2 ion channel pore whereas the secondary, low-affinity binding site can be attributed to the lipid face of the pore. These SPR results are in excellent agreement with the most recent solid-state NMR study of amantadine-bound M2 in lipid bilayers and provide independent support that the ion channel pore-binding site is responsible for the pharmacological activity elicited by the adamantane drugs.

adamantane drug resistance | surface plasmon resonance | viral ion channel | mutational analysis

As evidenced by recent H5N1 (avian) and H1N1 (swine) influenza outbreaks, the influenza A virus poses an ever-present global threat to human health. One of the initial responses in combating this disease involves the use of antiviral drugs such as the neuraminidase inhibitors oseltamivir and zanamivir. Whereas the efficacy of these drugs is well established, another class of approved antiviral drug known as adamantane M2 inhibitors (amantadine and rimantadine) has in the past been shown to be effective in treating seasonal influenza (1). Unfortunately, the emergence of several adamantane-resistant M2 mutations has severely curtailed the effectiveness of this class of drug to the extent that the Centers for Disease Control have recommended discontinuing its use (2). However, the recent flu outbreaks have demonstrably highlighted the immense benefit of having an effective antiviral treatment at hand, thereby reigniting the search for novel M2 inhibitors (3, 4).

The role of the influenza A M2 protein has been well documented. It forms a proton ion channel that operates early in the viral life cycle by facilitating the acidification of the endosomally entrapped virus, thereby enabling release of its RNA genome to allow viral replication (5). The M2 ion channel is 97 amino acids in size but it is the membrane-spanning portion (residues 22–46) that is required for its proton transport activity (6, 7) and its amantadine sensitivity (8). This transmembrane helix segment participates in the formation of tetramers (9) giving rise to an ion channel pore and it had been assumed that the adamantane-related compounds exerted their inhibitory effect by binding and therefore blocking this pore (8). Recently, two high-resolution structures containing the transmembrane portion of the M2 protein were simultaneously published. These structures were solved using X-ray crystallography (10) and solution state NMR (11) in the presence of amantadine and rimantadine, respectively. Each structure is globally similar, displaying a tetrameric helical bundle that forms an ion channel that is lined by polar residues (Fig. 1). Moreover, both structures elucidate the importance of the pH sensitive His37 and Trp41 residues that make up the channel gate at the base of the channel. The protonation state of the His37 residue in particular has been previously shown to play a critical role in proton channel gating (12–14). Differences between the two structures relate to the openness of the channel with the X-ray structure displaying an open state compared with the NMR structure that is in a closed conformation. The most striking and controversial difference, however, involves the location of the adamantane binding site, with the X-ray structure showing binding in the channel pore near the N terminus and the NMR structure reporting binding near the helix–helix interface of the tetramer near the C terminus (Fig. 1). This difference can in no way be regarded as subtle and cannot simply be attributed to the different-sized M2 peptide fragment used because both fragments have been shown to confer comparable folding, drug binding, and proton translocation properties (15). Subsequent studies have been published to shed light upon both binding modes (16–20) and recently, a solid state NMR (ssNMR) study by Cady et al. has shown that amantadine binding to both sites may exist (21).

A number of strategies have been used to probe the adamantane binding sites and some of these have included the substitution of key binding site amino acid residues, several of which are found in adamantane-resistant strains of the virus (17, 20, 22). Resistance to adamantane drugs develops both in vivo and in vitro and generally results from single point mutations in M2 involving residues 26, 27, 30, 31, and 34 (23, 24). Two residues, V27 and S31, are naturally dominant in vivo mutations and isolates bearing these mutations have increased alarmingly over recent years (25). Substitution of these two amino acids in adamantane structural and functional studies has yielded results suggestive of an ion pore-binding model. Mutation of residue D44 has little or no effect on amantadine inhibition (22) but has been identified in the solution NMR, lipid facing binding model as the residue responsible for binding with rimantadine (11). For this model, an unconventional allosteric mechanism has been proposed to rationalize the existence of the pore-lining adamantane-resistant mutants. Therefore the three residues, V27, S31, and D44, provide an ideal basis for examination of the M2 ion channel binding site.

Surface plasmon resonance (SPR) has been previously used to measure drug interactions to liposomes; however, its application in drug binding measurements to viral ion channels is more challenging with only two studies attempted. These studies involved

Author contributions: M.R.R. and M.G.C. designed research; M.R.R. performed research; M.R.R. and M.G.C. analyzed data; and M.G.C. wrote the paper.

The authors declare no conflict of interest.

*This Direct Submission article had a prearranged editor.

[1]To whom correspondence should be addressed. E-mail: marco.casarotto@anu.edu.au.

This article contains supporting information online at www.pnas.org/lookup/suppl/doi:10.1073/pnas.1002051107/-/DCSupplemental.

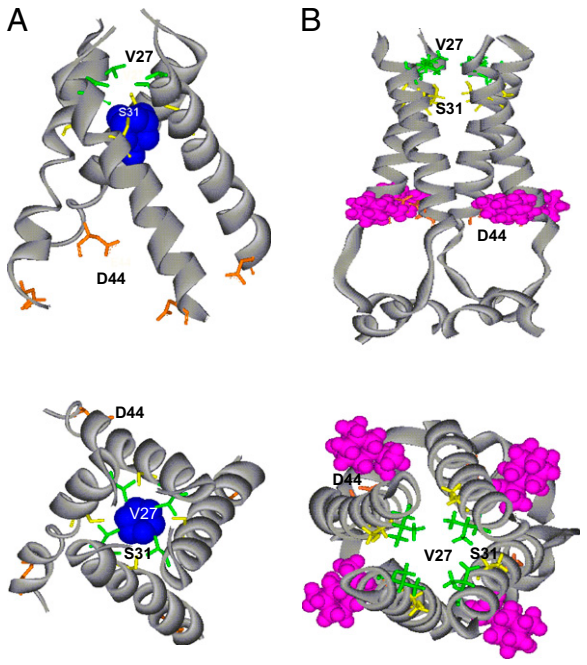

Fig. 1. Structures of the transmembrane domain of the influenza A M2 ion channel showing the adamantane binding sites. Key active-site residues are highlighted V27 (green), S31 (yellow), and D44 (orange). (*A*) Side and top–down view of the X-ray crystal structure of M2 (residues 22–46) bound to amantadine (blue) (3C9J) showing an ion-channel pore-binding site. (*B*) Side and top–down view of the solution NMR structure of M2 (residues 18–60) bound to rimantadine (magenta) (2RLF), showing a lipid-facing adamantane binding pocket.

amantadine binding to M2 ion channels (26) and protein E from the coronavirus responsible for severe acute respiratory syndrome (27). The binding of amantadine to the M2 ion channel, however, was found to be weaker than expected (by a factor of $\sim 10^3$), suggesting that this binding event may not be related to amantadine's inhibitory mode of action. Similarly, the binding affinity to protein E was extremely weak (7 mM) and comparable to binding of amantadine to empty liposomes. Here we investigate the binding of amantadine and rimantadine to small M2 peptides (residues 22–46) embedded in 1,2-dimyristoyl-sn-glycero-phosphocholine (DMPC) liposomes, using a modified SPR protocol. We identify a high- and a low-affinity binding site and use the three mutants, V27A, S31N, and D44A, to probe each of the two high-resolution binding site models proposed. We find that the high-affinity site correlates to the pore-binding model (X-ray model) whereas the low-affinity site can be ascribed to binding of the helix–lipid interface (solution NMR model). It is most likely that this latter site represents a peripheral binding event that is not related to the inhibitory mode of action associated with the adamantanes.

Results

The interaction of drugs with biological membranes and drug targets that reside in membranes is an important aspect of drug design. The accurate determination of drug binding affinities in such systems is crucial in understanding their pharmacological mode of action. The use of SPR as a tool to measure the drug binding affinities is well documented; however, measurements of drug binding to membrane-embedded proteins (in particular ion channels) presents a more challenging prospect. The viral ion channels or viroporins represent one of the smallest classes of ion channels and present an ideal opportunity to investigate drug binding to a protein in a membranous environment. The debate surrounding the mechanism of adamantane drug inhibition of M2 channel viroporins from influenza A also presents a perfect platform to showcase the capabilities of this technique. Here we use SPR to probe the mechanism of adamantane drug inhibition on M2 ion channels.

SPR Liposome Capture and Drug Binding Responses. The process of SPR events that include the liposome capture on the Biacore L1 sensor chip as well as the drug binding cycle is shown in Fig. 2*A*. The procedure involves the assembly of an artificial membrane surface by flowing M2 peptides embedded in DMPC liposomes over the chip surface until a maximal response is observed, indicating liposome saturation of the chip. This step is followed by the addition of PBS buffer to remove unbound liposomes and then injection of drug with subsequent measurement of the maximal response. The drug is then removed with PBS and the sensor chip is regenerated by cleaning with the isopropanol/HCl mixture.

Many drugs, particularly those that interact with membrane proteins, also have the potential to partition within membranes and it has been previously noted that amantadine interacts with membranes (28, 29). Using a protocol described by Abdiche et al. (30) [Eq. **1**], it was possible to accurately measure the affinity of these drugs to empty DMPC liposomes using SPR. For the adamantane drugs, Fig. 2*B* clearly shows a binding response at high drug concentrations and when analyzed, they were found to have a binding

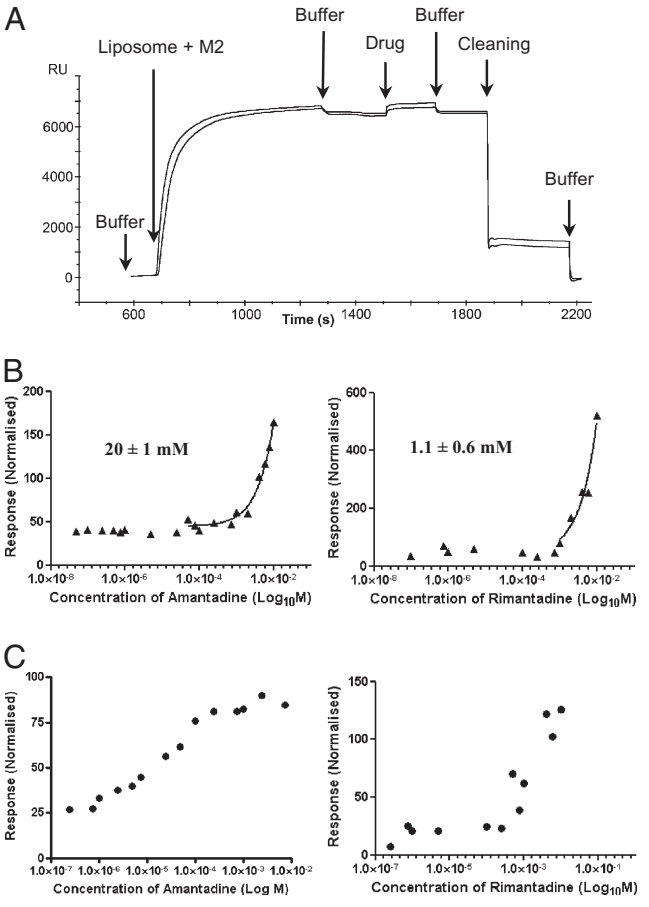

Fig. 2. SPR responses obtained for adamantane drug binding to DMPC liposome surface. (*A*) Typical sensorgrams for the complete liposome capture and drug binding cycle. (*B*) Binding response curves of amantadine and rimantadine to empty liposomes for the concentration range 0.01 μM to 10 mM. Mean binding-affinity values and their SDs are provided ($n = 3$ and 6 for amantadine and rimantadine, respectively). (*C*) Representative experiments showing a biphasic concentration–response curve for amantadine and rimantadine binding to the wild-type M2 ion channel peptides embedded in DMPC liposomes.

affinity of 20 mM and 1.1 mM for amantadine and rimantadine, respectively. In the case where the drug binding affinities to ion channels are comparable to the drug/liposome binding constants, both of these membrane interactions must be taken into consideration during the analysis and are included as K_{Dlipid} and $K_{Dpeptide}$ in Eq. **1**.

Upon the incorporation of the M2 peptides in the liposome preparation, a very different response profile was observed with addition of the adamantanes compared with the empty liposomes (Fig. 2*C*), suggesting that the M2 peptides had been successfully incorporated and that a specific binding event with the peptides had occurred. Figure 2*C* also shows that the amantadine/rimantadine-concentration responses to M2 ion channels under equilibrium conditions are biphasic in nature, indicating that two distinct binding events may be taking place. Analysis of SPR responses can be used to determine the stoichiometry of drug binding. However, because at high adamantane concentrations drug molecules are most likely displacing lipid molecules from the liposome, a direct stoichiometric comparison between the two binding events was not feasible. These two binding events were studied independently by examining the SPR responses at drug concentration ranges of 0.1–100 μM (low concentration) and 100 μM to 10 mM (high concentrations). Experiments were carried out at low concentrations for the wild-type strain of M2 (residues 22–46) as well as its M2 mutants V27A, S31N, and D44A. The data were fitted using Eq. **1** with representative binding curves displayed in Fig. 3 and the resultant binding affinities are summarized in Table 1. From these data, amantadine was found to bind wild-type M2 ion channels with a K_D value of 0.91 μM and the D44A mutant with a K_D value of 0.13 μM. In contrast, the V27A and S31N mutants can no longer support amantadine binding at these low concentrations. A complementary set of experiments was carried out with rimantadine and similar results to those for amantadine were observed (Table 1), i.e., K_D values of 0.38 and 0.77 μM for wild type and D44A, respectively, whereas no binding was observed for either V27A or S31N.

Analysis of data for the high amantadine concentration range (Fig. 4) resulted in a markedly different binding profile compared with the low concentration data. First, the binding affinity of amantadine was ≈450-fold weaker (0.40 mM) but more importantly, the D44A mutant did not support amantadine binding whereas the V27 AM2 mutant was found to bind with comparable affinity to the wild-type peptide, an outcome that is opposite to that observed at low amantadine concentrations. Analogous to the low concentration results, the S31N mutant was found not to bind amantadine. Importantly, the results observed at high concentrations for the wild-type and S31N, V27A mutants are remarkably similar to the results reported by Astrahan et al. (26), which are included in Table 2 for comparison. This is not surprising given that both studies were performed at a similar concentration range. The binding affinities of rimantadine at low and high concentration ranges were found to be comparable to those of amantadine (Tables 1 and 2) and indicate that the different binding sites proposed by the X-ray and solution NMR models cannot be attributed to the minor structural differences in the side chain of these two inhibitors. Whereas the weaker binding site affinities of the two adamantane drugs to wild-type M2 are similar, it should be noted that this weaker binding for rimantadine is only a factor of 2 stronger than rimantadine binding to liposomes. The rimantadine binding response curves at low and high concentrations are presented in Fig. S1.

Discussion

The publication of the high-resolution structures of the M2 ion channel/adamantane complexes (10, 11) has sparked great controversy in the drug design field with regard to the exact pharmacologically relevant binding site of these drugs to the M2 ion channel. The importance in resolving this issue has been highlighted in recent studies where both binding models have been used in drug molecular docking studies as the starting basis of a drug design strategy (17, 31). It had been assumed that the adamantane drugs, amantadine and rimantadine, bind in the pore region of the M2 ion channel by interacting with a series of pore-lining residues that include S31and V27 as depicted in Fig. 1*A*. Evidence supporting such an interaction is compelling and has been derived from wide-ranging sources that involved solid-state NMR (21, 32, 33), site-directed mutagenesis (19), and stoichiometric and functional studies (34). Indeed, when the structure of an amantadine/M2 complex was recently solved by X-ray crystallography (11), it was of no surprise that amantadine was reported to bind in the channel pore with many of the predicted amino acid residues V27, A30, S31, and G34 all found in close proximity to the amantadine molecule. However, in parallel with this study an NMR structure emerged that suggested that rimantadine bound to the outside of the M2 protein helices facing the lipid bilayer with residue D44 participating in a hydrogen bond interaction with rimantadine (Fig. 1).

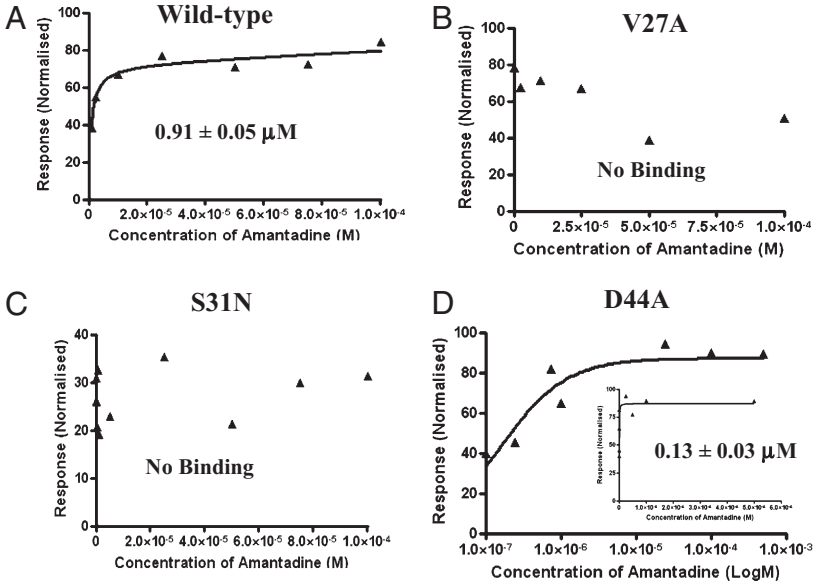

Fig. 3. Representative SPR dose–response curves for amantadine at low-concentration (0.1–100 μM) binding to M2 ion channels embedded in DMPC vesicles. (*A*) Wild type. (*B*) V27A. (*C*) S31N. (*D*) D44A (logarithmic concentration and *Inset* show standard concentration). Curves represent the equilibrium-binding data fitted to Eq. **1**. The mean equilibrium-binding affinity and SD for amantadine are displayed throughout. The term "no binding" refers to no specific binding to M2 ion channels.

Table 1. Binding constants of amantadine and rimantadine to M2 ion channels at low drug concentrations

	Amantadine			Rimantadine		
M2 variant	Binding affinity K_D, μM	SD, μM	*n*	Binding affinity K_D, μM	SD, μM	*n*
Wild type	0.91	0.054	6	0.38	0.028	6
V27A	NB	NB	6	NB	NB	6
D44A	0.13	0.025	3	0.77	0.062	6
S31N	NB	NB	3	NB	NB	6

NB denotes no specific binding to M2 ion channels.

Coexistence of Two Adamantane Binding Sites on M2. The SPR results indicate that two concentration-dependent binding events are taking place for both amantadine and rimantadine to the M2 ion channel. This is a critical finding and offers a logical explanation for the apparent discrepancy in the binding site observed between the X-ray and NMR structural data. The higher-affinity binding site for amantadine had a K_D of 0.91 μM at pH 7.5, which is of similar magnitude to that found in several earlier inhibitory studies (9 μM, ref. 34; and 2 μM, ref. 35). Confirmation of micromolar binding between amantadine and M2 ion channels in lipid bilayers has also been recently reported using isothermal calorimetry (15), where a slightly lower K_D value of 0.23 μM was measured in POPC/POPG bilayers.

An earlier SPR study also addressed the question of amantadine binding to M2 ion channels (26). In this study the affinity of amantadine to M2 was reported to be 360 μM, which is considerably weaker than the high-affinity value measured here or in any other published study. Careful examination of the conditions used in this study revealed a working amantadine concentration range of 0.07–10 mM, which is outside the range for higher-affinity binding measurements. Interestingly however, inspection of our data at this concentration range (Fig. 4*A*) suggests that a genuine binding event is taking place that, when analyzed, yields an almost identical binding constant (0.40 mM) to that previously measured by Astrahan et al. (26) (Table 2).

Mutational Analysis of the M2 Adamantane Binding Site by SPR. Our SPR results indicate that amantadine and rimantadine are capable of interacting with the M2 ion channel at two distinct sites with significantly different binding affinities. At low drug concentrations both the S31N and V27A mutants failed to bind the adamantanes whereas the D44A mutant facilitated binding to both amantadine and rimantadine with affinities comparable to or greater than that observed for the wild-type data. This result demonstrates conclusively that in our binding assay the absence of D44 does not preclude binding of the adamantanes. In fact, the binding affinity for amantadine is increased for this particular mutant, indicating that modification of D44 may allosterically influence the ion pore-binding site, thereby facilitating tighter inhibitor binding. Comparison of the binding profiles of the adamantane drugs at high concentrations reveals a very different binding profile for two of the mutants. At high adamantane concentrations the S31N and D44A mutants were found not to bind to M2 ion channels. The fact that at high concentrations the adamantanes do not bind the S31N mutant through the D44 residue provides additional support for an allosteric relationship between S31 and D44. Interestingly, an alternative interpretation of this allosteric relationship has been suggested by Pielak et al. to explain how the mutation of active-site residues abolishes binding to a remote site (20). At high concentrations, the mutant V27A is capable of binding the adamantanes with a similar affinity to the wild-type M2. Because the V27A variant is ada-

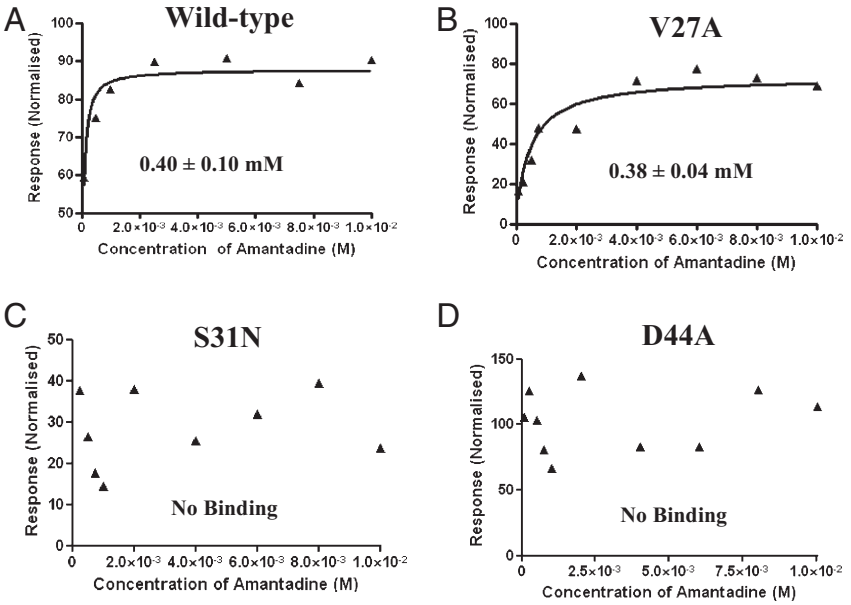

Fig. 4. Representative SPR dose–response curves for amantadine at high-concentration (0.1–10 mM) binding to M2 ion channels embedded in DMPC vesicles. (*A*) wild type. (*B*) V27A. (*C*) S31N. (*D*) D44A. Curves represent the equilibrium-binding data fitted to Eq. **1**. The mean equilibrium-binding affinity and SD for amantadine are displayed throughout. The term "no binding" refers to no specific binding to M2 ion channels.

Table 2. Binding constants of amantadine and rimantadine to M2 ion channels at high drug concentrations

	Amantadine			Rimantadine		
M2 variant	Binding affinity K_D, μM	SD, μM	*n*	Binding affinity K_D, μM	SD, μM	*n*
Wild type	400 (360)	100 (90)	3	500	150	3
V27A	380 (480)	37 (120)	3	810	270	3
D44A	NB	NB	3	NB	NB	3
S31N	NB	NB	3	NB	NB	3

The binding affinities displayed in parentheses were derived from an independent SPR study (26).
NB denotes no specific binding to M2 ion channels.

mantane resistant, it suggests that this lipid-binding face cannot alone act as the pharmacologically relevant binding site.

Location of the Adamantane Binding Sites of M2. Previous discussions in the literature concerning the M2 adamantane binding site locations have focused on the quality and validity of the X-ray and NMR data (19, 20, 36). However, the differences observed in binding site location could be attributed simply to the specific conditions associated with each of the two techniques. Examination of the experimental conditions (Table S1) shows differences in (*a*) the membrane solubilizing conditions, (*b*) pH conditions, (*c*) the type and concentration of inhibitor, and (*d*) the length of the M2 peptide. Each of these differences has the potential to influence where and how strongly the adamantane inhibitors may bind. This point is further demonstrated in a recent ssNMR study in which amantadine binding to M2 was found to occur at both sites in a concentration-dependent manner (21). Apart from the drug concentration, the ability to detect drug binding at both M2 binding sites may also depend on the other factors. For instance, the low temperatures used in ssNMR (243 K) may help reduce motional averaging experienced by the drug in the pore sufficiently to detect binding at this site. Alternatively, the micelle environment used by solution NMR could distort the M2 ion channel, not enabling the drug molecules to bind within the pore. All of these factors provide valid explanations for the variability associated with the detection of the adamantane binding sites. Similarly, it could also be reasonably argued that the diverse methods and different conditions (such as drug concentration) used for the M2 functional assays may explain some of the discordant results arising from these studies (17, 20, 37). It is interesting to note that there is good correlation between the high-binding-affinity SPR data with the results seen in influenza plaque assays and patch clamping experiments (17, 37) as well as between the liposomal flux assay (20) and the low-affinity SPR data (Table S2).

Due to its relatively uncomplicated setup, SPR is a technique capable of clarifying many of the inconsistencies detailed above. The presence of two concentration-dependent binding sites has also now been elucidated by ssNMR (21) and key elements of this study support our findings of high- and low-affinity sites. Nevertheless there are some important aspects of this work that are enhanced when viewed in conjunction with our SPR results. First, whereas the ssNMR study presents a comparative estimate of the two amantadine binding affinities (>40), our study provides a precise determination of these binding affinities revealing a difference of up to three orders of magnitude in binding. Second, through the mutational analysis, SPR suggests that an allosteric relationship may exist between the two binding sites. Finally, our SPR study provides confirmatory evidence that the D44 residue is a key residue implicit in low-affinity binding, which is in agreement with the ssNMR study (21).

Which Binding Mode Is Pharmacologically Relevant? The presence of these two distinct binding sites has raised the question of whether two modes of adamantane inhibition may be at work (38) and several key findings in this article shed light upon this issue. First, the fact that low-affinity binding of the adamantanes to V27A can still occur despite this mutant being adamantane resistant suggests that this site cannot independently inhibit M2 activity. Second, we have presented evidence of an allosteric relationship between the D44 and S31 residues of M2, allowing for the possibility that binding at the low-affinity site could synergistically influence the major pore-binding site. Approaching high adamantane concentrations, this cooperative binding event may account for some of the ambiguous results observed for some of the functional data (20). Importantly, however, on the basis of the very different SPR binding affinities of the two sites (0.91 vs. 400 μM for amantadine), it is highly likely that only the high-affinity pore site would be adequately populated on the basis of the steady-state plasma concentration recommended for these drugs [i.e., 300 ng/mL (~2 μM) for amantadine) (39). Furthermore, this last argument strongly suggests that the adamantane pore-binding site is responsible for its main pharmacological action and the lipid facing site represents a secondary binding site that is unlikely to be of any pharmacological relevance at the therapeutic dose used in a clinical setting.

In conclusion we have demonstrated using SPR that adamantane drugs are capable of binding M2 ion channels at two sites with binding site affinities differing by approximately three orders of magnitude. Using site-directed mutagenesis we have mapped the high-affinity binding site to the pore of the channel and the low-affinity site to a lipid facing pocket involving D44. On the basis of adamantane inhibitory studies, we conclude that the lipid facing pocket is not the primary site for the pharmacological action of adamantane drugs but rather represents a weaker secondary binding event that at artificially high drug concentrations may influence the inhibitory action of the principal pore-binding site.

Materials and Methods

M2 Peptide Synthesis and Purification. The wild-type M2 peptide (A/Udorn/72 strain) and its mutants were synthesized using solid phase chemistry on a Symphony/Multiplex multiple peptide synthesizer, using FMOC protection. Sequences are listed: (*i*) M2 WT SSDPLVVAASIIGILHLILWILDRL; (*ii*) M2 D44A SSDPLVVAASIIGILHLILWILARL; (*iii*) M2 S31N SSDPLVVAANIIGILHLILWILDRL; (*iv*) M2 V27A SSDPLAVAASIIGILHLILWILDRL.

Peptides were produced by Kerry McAndrew at the Bio-Molecular Resource Facility (BRF) at the Australian National University and received as a freeze-dried powder. A 10-mg quantity of peptide was dissolved in 5 mL of a 50/50 mixture of buffer A (Milli Q water with 0.1% trifluoroacetic acid) and buffer B (60% 2-propanol, 30% acetonitrile, 10% Milli Q water with 0.1% TFA) and then vortex mixed until dissolved before loading onto a C4 reverse phase HPLC column. Peptides were eluted from the column using a 40-min linear gradient from 20 to 100% buffer B and then lyophilized. The purity of the peptide was confirmed on an ABI 4800 MALDI TOF-TOF mass spectrometer.

Liposome Production. Liposomes were produced by organic solvent extraction using chloroform for the lipid components and trifluoroethanol (TFE) for the protein samples. The lipid component DMPC (Avanti polar lipids) was dissolved in chloroform at 10 mg/mL, placed in a round-bottomed flask, and evaporated by rotary evaporation at room temperature. For proteo-liposome

preparations, an appropriate amount of peptide dissolved in TFE was added to the liposome mixture, at a lipid to peptide ratio of 50:1, and the solvent was removed by rotary evaporation. To solubilize the lipid or proteolipid film, the mixture was dissolved in PBS, pH 7.4 (10 mM Na_2HPO_4, 137 mM NaCl), and incubated at 37 °C for 30 min with constant mixing. After solubilization, the crude liposome was freeze–thaw cycled between liquid nitrogen and a 40–50 °C water bath. To provide a uniform liposome sample, liposomes were extruded through a nitrogen powered extruder (Lipex Biomembranes), using a 0.1-μm Nucleopore cutoff membrane filter. Assessment of liposome size and quality was performed using dynamic light scattering measurements carried out on a Malvern Instruments Zetasizer Nano ZS. Electron microscopy images were also taken to confirm the formation of liposomes.

SPR. SPR measurements were performed on a Biacore 2000, using a carboxymethyl dextran-coated (L1) chip capable of binding liposomes. Running buffers were filtered through Whatman 0.2-μm PVDF membrane filters twice before beginning the experimental run, and drug solutions were filtered through a 0.2-μm syringe filter to remove any large aggregates. The L1 chip was cleaned before each experiment with a 50/50 mixture of isopropanol and 100 mM HCl and equilibriated with PBS buffer. After cleaning, the liposomes were immobilized over the chip (40 μL at a flow rate of 2 μL/min). Any excess of unbound liposome was removed by flowing 10 mM NaOH in PBS (10 μL at a flow rate of 20 μL/min) followed by PBS application for 4 min at a rate of 20 μL/min.

Binding experiments were carried out by injecting the adamantane drugs (60 μL at a flow rate of 20 μL/min) in the concentration range from 0.5 μM to 10 mM. Following the drug injection, the maximal response was noted and thereafter the drugs were allowed to dissociate for 1 min by application of PBS (at a flow rate of 20 μL/min). All binding assays were run overnight at a temperature of 20 °C. The results were analyzed with the Biaevaluation software (Biacore) and report tables were analyzed with Microsoft Excel using an in-house program, "divide and conquer." This program formats the data for export as well as allowing for normalization of the data relative to the amount of liposomes bound to the surface.

Because k_{on} and k_{off} rates of adamantane binding were extremely rapid, the binding analysis was based on equilibrium steady-state measurements, using maximal response values during the addition of the drug. The binding results were represented as concentration-response curves by fitting the data to Eq. **1**, using the program Graphpad Prism. Eq. **1** is adapted from the Biacore Biaevaluation software and includes two separate binding-affinity terms, K_{Dlipid} and $K_{Dpeptide}$ (30, 40) (in the case where drugs were bound to empty liposomes, the $K_{Dpeptide}$ component of Eq. **1** was not used):

$$\text{Response} = R_{max}\left(\frac{1}{(K_{DLipid}/[\text{Drug}]+1)}+\frac{1}{(K_{DPeptide}/[\text{Drug}]+1)}\right)+\text{Ns}\times[\text{Drug}]. \quad [1]$$

K_{DLipid} is dissociation constant to the empty liposome, $K_{Dpeptide}$ is dissociation constant to the ion channel, R_{max} is the maximal response, and Ns is any nonspecific interactions.

The quality of the fit was assessed by considering both the R^2 value and the SE. Typically, R^2 values were >0.90 and the SE <10%.

ACKNOWLEDGMENTS. We thank Prof. Nick Dixon and Llara Weaver for their technical advice and assistance. M.R.R. gratefully acknowledges a postgraduate scholarship from the Australian National University as well as generous support from Biotron Ltd. M.G.C. acknowledges funding support from the Australian Research Council.

1. Davies WL, et al. (1964) Antiviral activity of 1-adamantanamine (amantadine). *Science* 144:862–863.
2. Bright RA, et al. (2005) Incidence of adamantane resistance among influenza A (H3N2) viruses isolated worldwide from 1994 to 2005: A cause for concern. *Lancet* 366: 1175–1181.
3. Balannik V, et al. (2009) Design and pharmacological characterization of inhibitors of amantadine-resistant mutants of the M2 ion channel of influenza A virus. *Biochemistry* 48:11872–11882.
4. Wang J, et al. (2009) Discovery of spiro-piperidine inhibitors and their modulation of the dynamics of the M2 proton channel from influenza A virus. *J Am Chem Soc* 131: 8066–8076.
5. Helenius A (1992) Unpacking the incoming influenza virus. *Cell* 69:577–578.
6. Pinto LH, et al. (1997) A functionally defined model for the M2 proton channel of influenza A virus suggests a mechanism for its ion selectivity. *Proc Natl Acad Sci USA* 94:11301–11306.
7. Sakaguchi T, Tu Q, Pinto LH, Lamb RA (1997) The active oligomeric state of the minimalistic influenza virus M2 ion channel is a tetramer. *Proc Natl Acad Sci USA* 94: 5000–5005.
8. Hay AJ, Wolstenholme AJ, Skehel JJ, Smith MH (1985) The molecular basis of the specific anti-influenza action of amantadine. *EMBO J* 4:3021–3024.
9. Sugrue RJ, Hay AJ (1991) Structural characteristics of the M2 protein of influenza A viruses: Evidence that it forms a tetrameric channel. *Virology* 180:617–624.
10. Stouffer AL, et al. (2008) Structural basis for the function and inhibition of an influenza virus proton channel. *Nature* 451:596–599.
11. Schnell JR, Chou JJ (2008) Structure and mechanism of the M2 proton channel of influenza A virus. *Nature* 451:591–595.
12. Chen H, Wu Y, Voth GA (2007) Proton transport behavior through the influenza A M2 channel: Insights from molecular simulation. *Biophys J* 93:3470–3479.
13. Hu J, Fu R, Cross TA (2007) The chemical and dynamical influence of the anti-viral drug amantadine on the M2 proton channel transmembrane domain. *Biophys J* 93: 276–283.
14. Hu J, et al. (2006) Histidines, heart of the hydrogen ion channel from influenza A virus: Toward an understanding of conductance and proton selectivity. *Proc Natl Acad Sci USA* 103:6865–6870.
15. Ma C, et al. (2009) Identification of the functional core of the influenza A virus A/M2 proton-selective ion channel. *Proc Natl Acad Sci USA* 106:12283–12288.
16. Chuang GY, et al. (2009) Binding hot spots and amantadine orientation in the influenza a virus M2 proton channel. *Biophys J* 97:2846–2853.
17. Jing X, et al. (2008) Functional studies indicate amantadine binds to the pore of the influenza A virus M2 proton-selective ion channel. *Proc Natl Acad Sci USA* 105:10967–10972.
18. Khurana E, Devane RH, Peraro MD, Klein ML (2010) Computational study of drug binding to the membrane-bound tetrameric M2 peptide bundle from influenza A virus. *Biochim Biophys Acta*, 10.1016/j.bbamem.2010.03.025.
19. Ohigashi Y, et al. (2009) An amantadine-sensitive chimeric BM2 ion channel of influenza B virus has implications for the mechanism of drug inhibition. *Proc Natl Acad Sci USA* 106:18775–18779.
20. Pielak RM, Schnell JR, Chou JJ (2009) Mechanism of drug inhibition and drug resistance of influenza A M2 channel. *Proc Natl Acad Sci USA* 106:7379–7384.
21. Cady SD, et al. (2010) Structure of the amantadine binding site of influenza M2 proton channels in lipid bilayers. *Nature* 463:689–692.
22. Balannik V, et al. (2010) Functional studies and modeling of pore-lining residue mutants of the influenza a virus M2 ion channel. *Biochemistry* 49:696–708.
23. Boivin G, Goyette N, Bernatchez H (2002) Prolonged excretion of amantadine-resistant influenza a virus quasi species after cessation of antiviral therapy in an immunocompromised patient. *Clin Infect Dis* 34:E23–E25.
24. Hay AJ, Zambon MC, Wolstenholme AJ, Skehel JJ, Smith MH (1986) Molecular basis of resistance of influenza A viruses to amantadine. *J Antimicrob Chemother* 18(Suppl B): 19–29.
25. Deyde VM, et al. (2007) Surveillance of resistance to adamantanes among influenza A(H3N2) and A(H1N1) viruses isolated worldwide. *J Infect Dis* 196:249–257.
26. Astrahan P, Kass I, Cooper MA, Arkin IT (2004) A novel method of resistance for influenza against a channel-blocking antiviral drug. *Proteins* 55:251–257.
27. Torres J, et al. (2007) Conductance and amantadine binding of a pore formed by a lysine-flanked transmembrane domain of SARS coronavirus envelope protein. *Protein Sci* 16:2065–2071.
28. Li C, Yi M, Hu J, Zhou HX, Cross TA (2008) Solid-state NMR and MD simulations of the antiviral drug amantadine solubilized in DMPC bilayers. *Biophys J* 94:1295–1302.
29. Wang JF, Schnell JR, Chou JJ (2004) Amantadine partition and localization in phospholipid membrane: A solution NMR study. *Biochem Biophys Res Commun* 324: 212–217.
30. Abdiche YN, Myszka DG (2004) Probing the mechanism of drug/lipid membrane interactions using Biacore. *Anal Biochem* 328:233–243.
31. Du QS, Huang RB, Wang SQ, Chou KC (2010) Designing inhibitors of M2 proton channel against H1N1 swine influenza virus. *PLoS ONE* 5:e9388.
32. Cady SD, Mishanina TV, Hong M (2009) Structure of amantadine-bound M2 transmembrane peptide of influenza A in lipid bilayers from magic-angle-spinning solid-state NMR: The role of Ser31 in amantadine binding. *J Mol Biol* 385:1127–1141.
33. Yi M, Cross TA, Zhou HX (2009) Conformational heterogeneity of the M2 proton channel and a structural model for channel activation. *Proc Natl Acad Sci USA* 106: 13311–13316.
34. Wang C, Takeuchi K, Pinto LH, Lamb RA (1993) Ion channel activity of influenza A virus M2 protein: Characterization of the amantadine block. *J Virol* 67:5585–5594.
35. Zoidis G, et al. (2008) Design and synthesis of bioactive 1,2-annulated adamantane derivatives. *Org Biomol Chem* 6:3177–3185.
36. Stouffer AL, et al. (2008) The interplay of functional tuning, drug resistance, and thermodynamic stability in the evolution of the M2 proton channel from the influenza A virus. *Structure* 16:1067–1076.
37. Pinto LH, Holsinger LJ, Lamb RA (1992) Influenza virus M2 protein has ion channel activity. *Cell* 69:517–528.
38. Kozakov D, Chuang GY, Beglov D, Vajda S (2010) Where does amantadine bind to the influenza virus M2 proton channel? *Trends Biochem Sci,* 10.1016/j.tibs.2010.03.006.
39. Novartis (2007). Symmetrel [registered product information]. Available at www.novartis.com.au/PI_PDF/sym.pdf.
40. Nussio MR, Sykes MJ, Miners JO, Shapter JG (2007) Characterisation of the binding of cationic amphiphilic drugs to phospholipid bilayers using surface plasmon resonance. *ChemMedChem* 2:366–373.